Article:
Chen, Y., Liu, C., Yang, Y. et al. (2022) Flooding prognostic in packed columns based on electrical capacitance tomography and convolution neural network. IEEE Transactions on Instrumentation and Measurement, 71. 4504214. ISSN: 0018-9456

https://doi.org/10.1109/tim.2022.3184363

Convolutional Neural Networks Aided Electrical Capacitance Tomography for Flooding Prognostic in Packed Columns

Yuan Chen, Chang Liu, *Member, IEEE*, Yunjie Yang, *Member, IEEE*, Mathieu Lucquiaud and Jiabin Jia, *Senior Member, IEEE*

***Abstract*— The flooding of packed columns is accompanied by a steep increase in liquid hold-up and pressure drop, resulting in lower mass transfer efficiency and potential damage to equipment. This study aims to investigate, for the first time, the feasibility of Electrical Capacitance Tomography aided by Convolutional Neural Networks as an intensified alternative to conventional flooding prediction methods. Electrical Capacitance Tomography allows variations in the predominant characteristics of flooding events to be investigated in greater detail than in previous research. Aided by Convolutional Neural Networks, the Electrical Capacitance Tomography sensor enables high accuracy on liquid hold-up calculation and strong robustness against noise-contaminated measurements. In this work, a detailed comparison is made between liquid hold-up results using Convolutional Neural Networks and a more conventional Electrical Capacitance Tomography method based on Maxwell equation. Both methods can accurately calculate the liquid hold-up at low gas flow rates. The liquid hold-up predicted according to Maxwell equation did not match the measured values at high gas flow rates, showing discrepancies of up to 68%. In contrast, Convolutional Neural Networks is much superior to the Maxwell equation method at high gas flow rates, giving only 1% mean of difference than the reference liquid hold-up. Electrical Capacitance Tomography supported by Convolutional Neural Networks shows great fidelity for non-invasive monitoring of local liquid hold-up, allowing for more accurate, localized prediction of loading point and flooding point in packed columns.**

***Index Terms*—Electrical Capacitance Tomography (ECT); Flooding; Convolutional Neural Network (CNN); packed column; counter-current flow.**

I. Introduction

Post-combustion carbon capture technology has the important advantage of the ease of retrofitting onto existing power plants to enhance their efficiency with simultaneous carbon capture [1]. A major drawback of post-combustion carbon capture using chemical solutions is that the process requires extremely large equipment with difficulties in scaling down economically for industrial applications, such as refineries, steel making and fertilizers [2, 3]. Among the existing post-combustion carbon capture technologies, few focus on column design optimization that is essential for reducing the cost of investment in the capture process. It can be achieved either by developing new high-performance packing or an adequate design of packed columns [4].

A packed column is the critical equipment used for post-combustion technologies. It has received much attention due to its high capacity, lower cost and high efficiency. Random and structured packings are commonly used in industry to improve contact surface area between two phases, i.e., gas and liquid, in the absorption process to maximize separation efficiency. However, flooding occurs in packed columns when either the gas or liquid flow is increased beyond the capacity of the column, accompanied by a sharp increase of the pressure drop, loss of mass transfer efficiency, and heavy entrainment [5].

Terms used for explaining flooding mechanisms:

1) Loading point: At the loading point of a column the gas velocity is high enough to destabilize the liquid film and influence the liquid flow. After this point, the liquid will accumulate in the column and lead to higher liquid hold-up and higher pressure drop until flooding happens.
2) Flooding point: Flooding point is the upper limit of the packed column operation. At this point, there is an excessive accumulation of liquid in the entire packed column.
3) Liquid hold-up: Liquid holdup is a hydrodynamic property and is defined as the ratio of the volume of a packed column occupied by the liquid to the total volume of the packed column.
4) Local liquid hold-up: In this paper, the local liquid hold-up is defined as the liquid hold-up at ECT measured area.

Flooding points, as an indication of the upper capacity limit of a packed column, will affect packed column design. In a counter-current packed column, operating in the loading zone between the loading and flooding points is recommended, to achieve a good mass transfer rate [6]. Therefore, a counter-current packed column is generally designed to 70-80% of the flooding point velocity [6-8], a lower boundary of 60% was also proposed for safety concerns [9]. This practice provides

Information on the data supporting the results presented here, including how to access them, can be found in the University of Edinburgh data repository <https://doi.org/10.7488/ds/3151>. We thank Mr. Derek Watson, Mr Douglas Halley and Mr Douglas Carmichael for technical support. *(Corresponding author: Chang Liu.)*

Chen. Y, Liu. C, Yang. Y, Lucquiaud. M and Jia. J are with the School of Engineering, University of Edinburgh, Edinburgh EH9 3JL, U.K. (e-mail: C.Liu@ed.ac.uk).

sufficient margin to (a) allow uncertainties associated with the prediction of the flooding point and (b) to keep the designed point away from the region where efficiency rapidly diminishes (just below the flooding point). However, this practice results in the oversizing of packed column diameters, and thus a decrease in efficiency. In the past decade, several empirical or semi-empirical correlations have been developed to determine the loading and flooding points and liquid hold-up and pressure drop in the pre-loading and loading zones for either random or structured packing [10-13]. However, these authors have identified a wide variation between various correlations.

To take advantage of the improved performance of these packings, accurate prediction of the hydrodynamic capacity would allow operation closer to flooding velocity and thus reduce the capital costs of the packed column. Two major process variables can be measured in a packed column for online flooding prognosis, i.e., pressure drop and liquid hold-up. A majority of the state-of-the-art methods measure pressure drop, which shows a significant increase when flooding is about to happen. However, online flooding detection by intrusive pressure transducers can cause a delay in reaction as a complete curve of pressure drop is required to identify accurately the loading point and flooding point. The alternative to identify flooding is to monitor the increase in liquid hold-up in the packed column [14]. In previous studies on packed column flooding, only the global pressure drop or global liquid hold-up has been measured, between the packed column liquid inlet and outlet. Since measurement of global liquid hold-up by draining the packed column is unrealistic, visualization of the reactive process in the packed column has been used for online packing monitoring [15]. To implement this visualization technique, a packed column with a transparent pipe is applied for the safe operation of the packed column close to the flooding point.

Radiation-based tomographic techniques can image the cross-sections of the packed column at different axial positions [16], providing information on liquid hold-up, hydrodynamic liquid spreading patterns of rotating packed beds [17, 18], bubbling fluidized beds [19] and counter-current flow distillation columns [16]. However, the shortcomings in radiation-based tomography include radiation hazards and expensive equipment. Therefore, this method cannot be used in a normal industrial environment. As a non-radiative, non-invasive, fast and low-cost tomographic modality, the application of electrical capacitance tomography (ECT) has been recently initialized to study the multiphase flow [20, 21]. For example, ECT was employed by Wongkia et al. [22] to study the flooding capacity of counter-current flow in inclined packed columns filled with random packings. Strazza et al. [23] used a simple 2-electrode capacitance sensor for liquid hold-up measurement in core-annular flows. Various recent studies have shown that an ECT system can measure the liquid flow distribution and thus obtain the velocity measurement of two-phase flows [24, 25]. Several studies have used ECT to better understand the hydrodynamics of co-current flow in packed columns [26], dynamic liquid distribution in a fixed bed column [27] and monitor gas voids in a packed bed column [28]. Recently, Li et al. [29] used ECT to demonstrate a new flooding index for packed column flooding monitoring that enabled timely warning of the occurrence of flooding.

With the rapid development of machine learning algorithms, data driven ECT techniques have been validated for the analysis of multiphase flow in many applications. For example, Jin et al. [30] used a deep learning-based method to accomplish image reconstruction in ECT. Chen et al. [31] used a multiple measurement vector model-based learning algorithm to solve the multifrequency electrical impedance tomography image reconstruction problem. Grzegorz et al. [32] used the long short-term memory network to intelligent selection of the best image reconstruction methods depending on the reconstructed case. Compared with traditionally computational image reconstructions, machine learning algorithms could take advantage of multiple input parameters and massive data. However, ECT sensor suffers a nonlinear behavior, particularly for high permittivity media such as water and a thick pipe wall [33]. The image reconstruction procedure may suppress quite a good amount of information from the capacitance data and lead to unreliable results. Therefore, many researchers have tried machine learning aided ECT methods to directly mapping the relationship between ECT measurements and multiphase flow hydrodynamic parameters to bypass the image reconstruction. Zainal-Mokhtar and Mohamad-Saleh [34] used a multilayer perceptron artificial neural network to directly estimate oil fraction in a pipe with normalized capacitance measurements. Wang and Zhang [35] used support vector machines (SVM) to identify the flow regime of two-phase flows. Hasan et al. [36] concluded that the Convolutional Neural Network (CNN) outperformed the SVM classifier in terms of testing accuracy. These works indicated that machine learning possibly used to the online measurement for liquid hold-up estimation without image reconstruction. To date, a CNN has been employed to explore the relationship between ECT measurements and the permittivity distribution [37]. Compared with conventional method the main advantage of CNN is that it automatically detects the important features from capacitance measurements without any empirical parameter and selection of the measurement path. They also show strong robustness when addressing the ECT inverse problems that are inherently nonlinear and ill-posed [33, 38, 39].

Built on our previous ECT research on flooding monitoring [29], a novel CNN-based ECT technique is developed in this work and, for the first time, applied to the characterization of flooding prognostic against experimental data. Instead of monitoring the global variables such as global liquid hold-up and global pressure drop, this development enables accurate monitoring of the local variations of liquid hold-up under flooding conditions, thus indicating quantitatively the dependence of local liquid hold-up in a packed column on the process parameters, such as the gas superficial velocity.

Measurement of the local liquid hold-up in a flooded packed column using the ECT sensor has two challenges: The first challenge is the flow regime transition involved in the flooding phenomenon. The gas phase dominant laminar flow is expected to become liquid phase dominant turbulence flow at a high gas flow rate. Therefore, ECT must operate with a liquid phase dominant absorption mass transfer operation to monitor flooding. However, ECT remains unreliable for measuring liquid phase dominant absorption mass transfer operation as the error for the ECT modality starts to increase sharply at 60% liquid hold-up [40]. Secondly, the position of the ECT sensor must be adjusted appropriately to monitor the relationship between local liquid hold-up and flooding.

To address these challenges, a flooding monitoring strategy using CNN-aided ECT is proposed. A portable ECT sensor is employed for free movement in the longitudinal direction of the packed column. At each axial position, all pressure drop, liquid hold-up and flow information data are simultaneously recorded at the same sampling rate using LabVIEW program at the lab-scale test rig. This study shows that the flooding can be earlier measured by local liquid hold-up than global liquid hold-up or pressure drop. Compared with the conventional liquid hold-up calculation model, the newly introduced CNN-aided method is more accurate, especially for data from high gas flow rates.

In the rest of this paper, the ECT system and a conventional liquid hold-up calculation model are introduced in Section II A and Section II B. Subsequently, CNN architecture is established using the ECT and reference liquid hold-up in Section III. Then, the experimental setup and campaign are described in Section IV. Predicted liquid hold-up obtained from ECT as well as loading points and flooding points derived from the CNN-aided method are presented, with the accuracy of the model discussed in Section V. Finally, a brief conclusion is presented in Section VI.

II. Methodology

A. Fundamentals of Electrical Capacitance Tomography

In our study, capacitances are recorded using an eight-electrode ECT sensor, which is installed at a packed column. The measured capacitances are used to retrieve the cross-sectional permittivity distribution within the sensing area based on a pre-calculated sensitivity map. For the forward problem of ECT, the linearized model describing the relationship between normalized capacitance data C_{norm} and the normalized permittivity change g is given by:

$$C_{norm} = Sg \quad (1)$$

where S is the matrix giving a sensitivity map for each electrode pair. Therefore, the inverse problem of ECT is to calculate the relative permittivity distribution from the measured capacitances. Common image reconstruction algorithms can be referred to in Yang and Peng [41]. Modified Sensitivity Back-Projection (MSBP) algorithm is used for ECT image reconstruction [42].

The ECT system used in this work, as shown in Fig. 1, includes an ECT sensor, a data acquisition system and a computer with ECT imaging software [43]. The ECT sensor contains 8 electrodes of 7.5 cm width and 10 cm length made from copper foil. They are mounted on the outer surface of the packed column and covered by an earthed shield electrode. The excitation signal is a sinusoidal wave with 14 Vp-p at 200 kHz. The data acquisition system digitizes the voltage signals sampled from the electrodes, which are then transferred to the computer through USB communication. The data collected by the proposed measurement system can be used for real-time imaging at a frame rate of 714 frames per second (fps).

B. Electrical Capacitance Tomography sensor calibration and liquid hold-up calculation

Recent studies have shown that either the two-end or the single-end calibration methods can be used for normalizing the measured capacitances [44]. For the two-end calibration method, the ECT was calibrated between the lowest and the highest permittivity limits. The intermediate pre-pixel normalized capacitance at each measured projection under the condition of gas-liquid flow is given by:

$$C_{norm} = \frac{C_{mea(j)} - C_{l(j)}}{C_{H(j)} - C_{l(j)}}, j = 1,2,\dots,N \quad (2)$$

where j is the electrode pair, N is the maximum number of measurements. $C_{mea(j)}$ is the measured capacitance at the j^{th} location. $C_{l(j)}$ and $C_{H(j)}$ are the reference capacitances at the j^{th} location when the sensing field is full of low permittivity media (air) and high permittivity media (water), respectively. For the two-end calibration method, the full calibration with high permittivity media is impractical in industrial applications as it requires the column cross-section to be filled with water. Therefore, the single-end calibration method is used in this work, in which single reference media is only needed [44]. The single-end normalization model is expressed as:

$$C_{norm} = \frac{C_{mea(j)}}{C_{ref(j)}}, j = 1,2,\dots,N \quad (3)$$

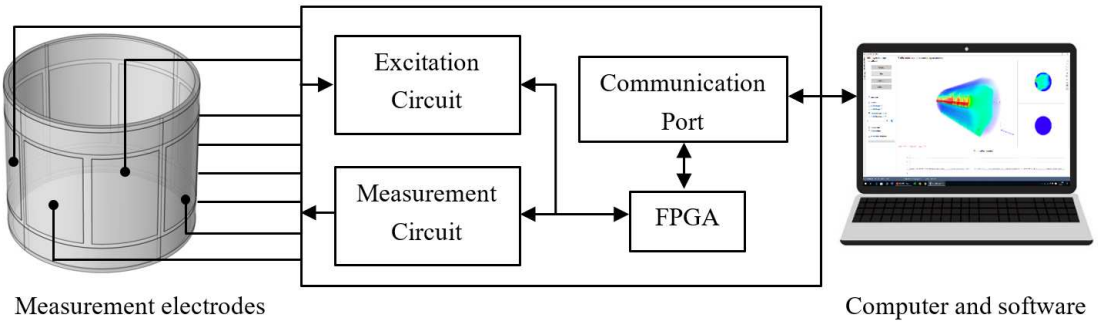

Fig. 1. Schematic diagram of the ECT system

where $C_{ref(j)}$ is the reference capacitance when the packed column is full of low permittivity media, i.e., air with packing. However, this reference capacitance is not constant: it is affected by the wetting and pre-flooding of the packing.

Under a linear approximation, the relationship between permittivity distribution and the measured capacitance is expressed as:

$$\frac{C_{mea(j)}}{C_{ref(j)}} \approx \frac{\sum_{k=1}^{w} \varepsilon_{mea(k)} s_{j,k}\left(\varepsilon_{mea(k)}\right)}{\sum_{k=1}^{w} \varepsilon_{ref(k)} s_{j,k}\left(\varepsilon_{ref(k)}\right)} \quad (4)$$

where k is the pixel number of the sensitive field and w is the maximum number of pixels. The measured and reference permittivity at the k^{th} pixel is represented by $\varepsilon_{mea(k)}$ and $\varepsilon_{ref(k)}$, respectively. The sensitivity matrix S can be calculated using the finite element method (FEM) in advance. The element $s_{j,k}$ of the normalized sensitivity matrix denotes the mapping relationship between the j^{th} projection and the k^{th} pixel in the image. The ratio between $\varepsilon_{mea(k)}$ and $\varepsilon_{ref(k)}$ can be approximated as follows:

$$\frac{\varepsilon_{mea(k)}}{\varepsilon_{ref(k)}} \approx \frac{\sum_{j=1}^{N} \frac{C_{mea(j)}}{C_{ref(j)}} s_{j,k}\left(\varepsilon_{mea(k)}\right)}{\sum_{j=1}^{N} s_{j,k}\left(\varepsilon_{ref(j)}\right)} \quad (5)$$

The phase permittivity variations due to phase fraction change are given by Ramu-Rao mixing law [45]. This correlation can be applied when an immiscible two-phase flow is homogeneous, and the low permittivity phase is continuous [46]. Thus, the permittivity of the two-phase mixture $\varepsilon_{mixture}$ can be obtained from the high permittivity phase in mixture ratio (HMR):

$$\varepsilon_{mixture} = \varepsilon_{gas} \frac{1+2HMR}{1-HMR} \quad (6)$$

where ε_{gas} is the permittivity of gas phase. There are three media in the packed column, i.e., air, water and plastic packing. The relative permittivity of water is approx. 80, which is much larger than that of plastic packing approx. 2, that of air approx. 1. Based on Maxwell equations [44], the liquid hold-up h_L in the homogeneous flow with the three media can be obtained by:

$$h_L \approx \frac{\varepsilon_{mea(k)} - \varepsilon_{ref(k)}}{\varepsilon_{mea(k)} + 2\varepsilon_{ref(k)}} \approx \frac{\varepsilon_{mea(k)}/\varepsilon_{ref(k)} - 1}{\varepsilon_{mea(k)}/\varepsilon_{ref(k)} + 2} \quad (7)$$

The method for liquid hold-up calculation can be used across different packed column zones with different flow patterns. However, it has previously been reported that the error of ECT starts to increase sharply at 60% liquid hold-up [40]. We expect this Maxwell equation-based method to be appropriate with gas phase dominant flow at low gas flow rates, but that it will inevitably cause large errors when the packed column is flooding.

Equation (8) and (9) are used for the reference liquid hold-up calculation. In the pre-loading zone, the local liquid hold-up $h_{L,local}$ can be derived from (8), by assuming homogeneous and equal velocities at packing sections.

$$h_{L,local} \approx h_{L,global} \approx \frac{V_{ref} - V_{mea}}{V} \quad (8)$$

where $h_{L,global}$ is the global liquid hold-up derived from the level meter. V_{ref} and V_{mea} are the reference liquid volume and the online measured liquid volume at the water tank. V is the volume of the whole packed column.

In the loading zone, it can also be reasonably assumed that the liquid starts to accumulate at the bottom section only and there is no obvious change of liquid hold-up at the rest of the packing sections. The local liquid hold-up at the loading zone can be derived from (9).

$$h_{L,local} \approx h_{L,loading} + \frac{V_{mea} - V_{loading}}{V_{ECT}} \quad (9)$$

where $h_{L,loading}$ is the local liquid hold-up at the loading point. $V_{loading}$ is the level meter measured liquid volume at the water tank and V_{ECT} is the volume of a section of packed column covered by ECT.

III. Convolutional Neural Networks-Aided Electrical Capacitance Tomography for Flooding Prognostic

For more accurate and faster predictions of flooding, we developed a CNN-based model to map the relationship between ECT data and liquid hold-up directly. CNN has some distinct advantages in image processing: Local connections and shared weights enable CNN to detect useful feature patterns with less pre-processing than other image classification algorithms [39]. This means CNN can learn to optimize its internal parameters or kernels through automated learning [47]. This subsection uses the CNN-aided ECT method for local liquid hold-up calculation and, hence, flooding prediction.

A. Dataset Construction

The first step in the dataset construction is to collect the flooding data for all the packed column experiments. The data from two scenarios, i.e., ECT installed on the bottom and top sections, are collected. When the flow pattern of the process is stable, a large amount of repeated data will be collected, which will possibly lead to overfitting. Only the most important section containing information about transients in the process is used [48]. The second step is to identify appropriate flooding indicators. Based on a previous study by some of the authors,

	1	2	3	4	5	6	7	8
1	C_{1-1}	C_{1-2}	C_{1-3}	C_{1-4}	C_{1-5}	C_{1-6}	C_{1-7}	C_{1-8}
2	C_{2-1}	C_{2-2}	C_{2-3}	C_{2-4}	C_{2-5}	C_{2-6}	C_{2-7}	C_{2-8}
3	C_{3-1}	C_{3-2}	C_{3-3}	C_{3-4}	C_{3-5}	C_{3-6}	C_{3-7}	C_{3-8}
4	C_{4-1}	C_{4-2}	C_{4-3}	C_{4-4}	C_{4-5}	C_{4-6}	C_{4-7}	C_{4-8}
5	C_{5-1}	C_{5-2}	C_{5-3}	C_{5-4}	C_{5-5}	C_{5-6}	C_{5-7}	C_{5-8}
6	C_{6-1}	C_{6-2}	C_{6-3}	C_{6-4}	C_{6-5}	C_{6-6}	C_{6-7}	C_{6-8}
7	C_{7-1}	C_{7-2}	C_{7-3}	C_{7-4}	C_{7-5}	C_{7-6}	C_{7-7}	C_{7-8}
8	C_{8-1}	C_{8-2}	C_{8-3}	C_{8-4}	C_{8-5}	C_{8-6}	C_{8-7}	C_{8-8}

Fig. 2. An example of Electrical Capacitance Image obtained from the 8-electrode ECT sensor.

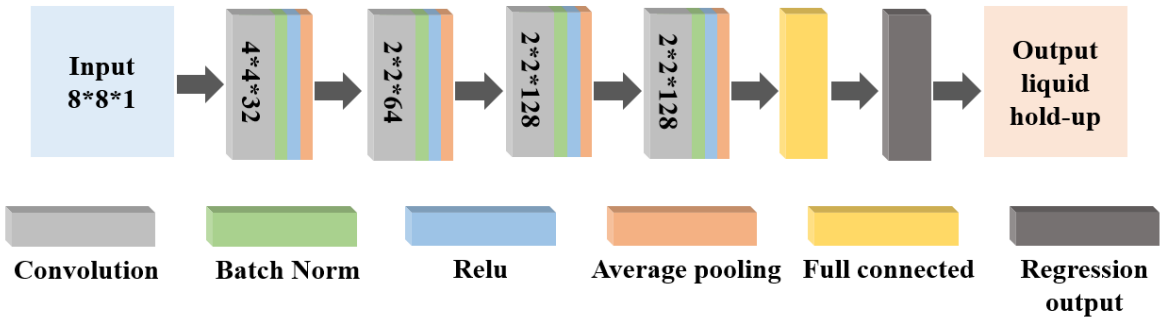

Fig. 3. Schematic of a CNN structure for flooding prediction

TABLE I: UNITS FOR MAGNETIC PROPERTIES HYPERPARAMETERS OF CNN IMPLEMENTED IN THIS WORK

Layer	Input dimension	Output dimension	weight matrix size	Stride	Padding
Conv1	8×8×1	5×5×32	4×4	(1,1)	0
Average pool 1	5×5×32	2×2×32	2×2	(2,2)	0
Conv 2	2×2×32	2×2×64	2×2	(1,1)	0
Average pool 2	2×2×64	2×2×64	2×2	(2,2)	0
Conv 3	2×2×64	2×2×128	2×2	(1,1)	0
Average pool 3	2×2×128	2×2×128	2×2	(2,2)	0
Conv 4	2×2×128	2×2×128	2×2	(1,1)	0
Average pool 4	2×2×128	2×2×128	2×2	(2,2)	0
Fc 1	512	1	2×2	-	-

the ECT measured capacitance can be a good indicator of flooding for the packed column [29]. Other variables, e.g., pressure drop and global liquid hold-up, measured during the process will be used for comparison.

An operating liquid load of 21.17 m^3/m^2h is used for all test conditions. The operating temperature is approximately 20 ^oC at 1.01 bar. Gas flow velocities from a minimum value of 1.11 m/s up to 6.89 m/s are tested to collect the data from the full range of available conditions to avoid data selection bias. The liquid hold-up will constantly change as the gas flow velocities increase incrementally at ECT measured location. The liquid hold-up data are collected over 30 seconds at a rate of 10 Hz. For each scenario, a total of 35 sets of different air flow rates are generated, each set with 300 samples. Therefore, a dataset with a total of 10,500 samples is created. We adopt the basic ECT measurement strategy [49] and a completed measurement cycle containing 28 capacitance measurements. Each sample contains an 8*8 Electrical Capacitance Image (ECI) which represents capacitance measurements and a true local liquid hold-up derived from level meter measurements using (8) and (9). Fig. 2 shows an ECI of capacitance distribution. Each ECI is mapped by the normalized 56 capacitance measurement with the rest padded with 0 [39]. For each capacitance value, the left number on subscript corresponds to the excitation electrode, while the right one corresponds to the measurement electrode. Capacitance measurement $C_{1\text{-}2}$ is assumed to be the same as $C_{2\text{-}1}$. Therefore, the 28 capacitance measurements are doubled to 56 capacitance measurements. Cells with the same number on subscript are padded with 0, e.g., $C_{1\text{-}1}$, because an electrode is not possible to work as an excitation electrode and measurement electrode at the same time. The data from each scenario is randomly divided into a training set with 8,925 samples and a test set with 1,575 samples. The training data set is used to develop the CNN-aided liquid hold-up predictors while the test data set is used to evaluate the predictors.

B. Network architecture

Then, CNN is established to predict the local liquid hold-up using the network structure shown in Fig. 3. The CNN contains four convolution layers, four average pooling layers and a fully connected layer. The input is the capacitance measurements with dimensions of 8*8*1. The real-time local liquid hold-up values are calculated as reference labels. ECT training data with liquid hold-up labels is pretreated by using the average method because capacitance and liquid hold-up is collected at different frequencies. The weight matrix size of the kernel function is chosen as 2*2 due to the small size of the input data. The depth of the convolution layer increases from 32 and ends up with 128. Finally, a regression layer is connected to the output of the

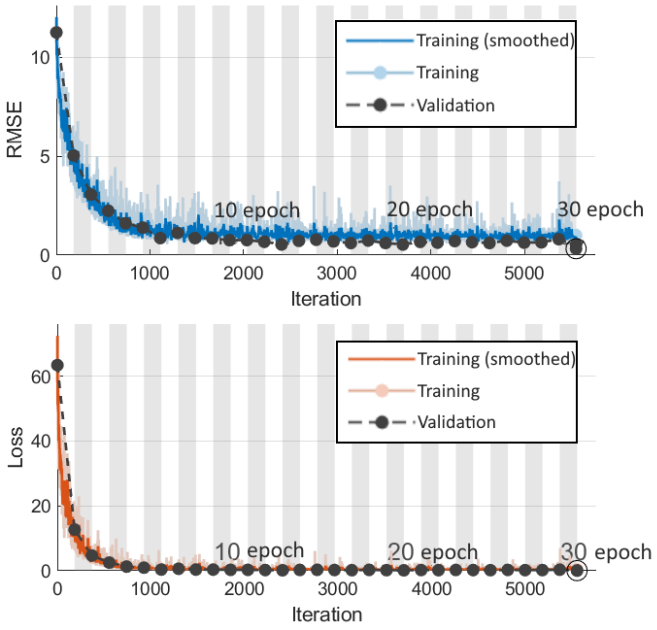

Fig. 4. Training and validation curves.

fully connected layer, performing as the final output layer of the CNN, that is, the predicted liquid hold-up. Detailed hyperparameters of the CNN is shown in Table 1.

C. Training

We represent the input ECI as c, the output liquid hold-up as $\widehat{h_L}$, and the network CNN-ECI as $f(\cdot;\theta)$, where θ denotes the hyperparameters of CNN-ECI. c can be mapped to $\widehat{h_L}$ by $f(\cdot;\theta)$:

$$\widehat{h_L} = f(c;\theta) \tag{10}$$

$\widehat{h_L}$ is expected to be as close as possible to the reference liquid hold-up h_L. This purpose can be achieved by adjusting θ to minimize the loss function $E(c, h_L;\theta)$:

$$E(c, h_L;\theta) = E\|h_L - f(c;\theta)\|_2^2 \tag{11}$$

To avoid overfitting, an L_2 regularization term is added as a weight to the loss function $E(c, h_L;\theta)$ [50]. The weighted loss function with the L_2 regularization term is derived from the equation:

$$E_R(c, h_L;\theta) = E(c, h_L;\theta) + \lambda\Omega(w) \tag{12}$$

where w is weight vector, λ is regularization coefficient. The regularization function $\Omega(w)$ is given by:

$$\Omega(w) = \frac{1}{2}w^T w \tag{13}$$

Stochastic gradient descent with a momentum (SGDM) algorithm [50] is employed to optimize the networks in this work. The initial learning rate is 10^{-5}. L_2 regularization is employed to prevent the networks from overfitting with the penalty factor set as 10^{-5}. The training and validation loss curves are shown in Fig. 4, where RMSE is the root mean square error of the predicted liquid hold-up. The number of training epochs depends on the degree of complexity of experiments. In this experiment, the number of epochs is set as 30 for adequate convergence. The batch size of each update is 128. The smallest validation loss appears at the 8th epoch. When trained with more epochs, the validation loss converges at a slightly higher value, meaning that the network is overfitted. The network is implemented with Deep Learning Toolbox (14.1) in Matlab (R2020b) on a computer with an Nvidia 1660 Ti GPU.

IV. Experimental Setup and Campaign

The packed column test rig shown in Fig. 5 is used to simulate a lab-scale counter-current absorption carbon capture application. The experimental rig is made of a transparent glass pipe to visually observe the flooding phenomenon in the column [51]. The packed column dimensions were internal diameter r_i = 190 mm; external diameter r_e = 200 mm, height h = 1130 mm. The packed column has been tested using polypropylene structured packings Mellapak 250.Y from Sulzer Chemtech Ltd. Four sections of 180 mm diameter packing with height equal to 315.0 mm, 157.5 mm, 157.5 mm and 315.0 mm were equipped in the packed column from bottom to top. As specified by the manufacturer, the packings have a low volume fraction, approximately 12%, in the column.

The column is operated in a counter-current flow configuration. The liquid from a water tank is supplied to the liquid distributor using a pump with an electronic controller and an OMEGA FMG71B-A-BSP magnetic inductive flow meter with an accuracy of ± 2.0%. Air from two Windjammer 119153 air blowers is injected into the column filled with structured packing through an air distributor at the bottom of the column to allow gas to flow into the column uniformly. The air flow rate is regulated by a voltage controller and measured by a TSI AIRFLOW TA465 MULTIFUNCTION ANEMOMETER with an accuracy of ± 3.0%. For a given liquid flow rate, the gas flow increases incrementally from a minimum value of 1.11 m/s up

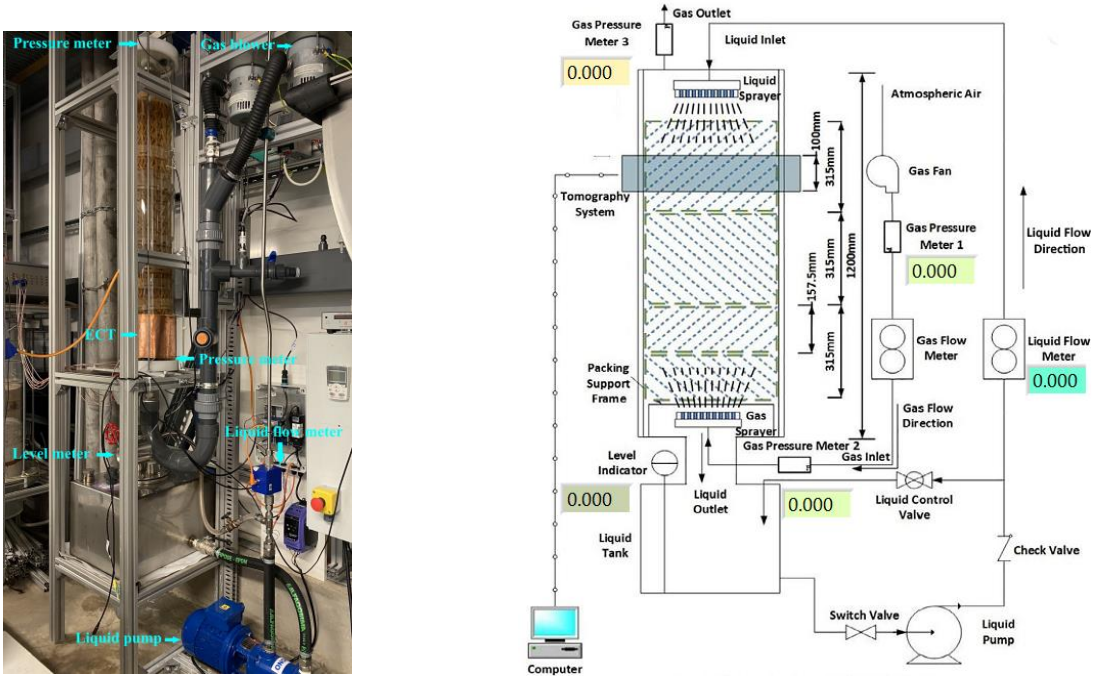

(a) (b)

Fig. 5. Counter-current packed column experimental set up (a) photo and (b) schematic diagram reprinted from [36]

to 6.89 m/s. Two Cole-Parmer T-68075-10 pressure transducers, with a precision of ± 0.25%, are placed at the top and bottom of the column where the gas flow and liquid flow are introduced to the packed column. A WIKA FLM-S Magneto strictive level transmitter with an accuracy of ± 0.5 mm is used to monitor the amount of liquid inside the water tank. By accounting for the liquid inventory staying in the piping of the system, the global liquid hold-up can be calculated. The measured liquid hold-up is then used to verify the liquid hold-up calculated by Maxwell equations.

Before the experiments, the ECT sensor is calibrated with an empty pipe. In the experiments, the ECT sensor is positioned firstly at the bottom and then at the top of the column, as shown in Fig. 9 (a) and Fig. 14 (a), respectively. Pressure differential readings are taken using the two pressure transducers placed at the top and bottom of the column, respectively. The level transmitter placed in the water tank is used to estimate the global liquid hold-up within the region where the ECT sensor is mounted. In all experiments, the packed column is operated at a constant liquid flow rate (21.17 m^3/m^2h) whereas the gas flow rate is increased in the minimum increment until the column is flooded. The gas flow rate is changed every 3 minutes to ensure the flow pattern is stabilized after the change of the gas flow rate. Therefore, the data are acquired simultaneously using the ECT sensor, the pressure sensor, and the level meter for both unsteady-state and steady-state flows. The sampling frequencies of ECT is 714 fps. The sampling frequencies of pressure sensors, flow meters and the level meter are 10 Hz.

V. Results and Discussion

ECT measurements are first used to reconstruct the liquid distributions. Then, the reconstructed distributions are used to compute the local liquid hold-up by using the Maxwell equation. The benefit of the CNN method is that it could directly predict the local liquid hold-up without image reconstruction. Reference measurements of liquid hold-up are available at the test rig. This allows the liquid hold-up calculated by the Maxwell equation and the CNN method to be compared with the true liquid hold-up. The effect of gas flow on the pressure drop and liquid hold-up can be analyzed based on experiment results. The ECT is installed on the top and bottom to measure the local loading point. Local loading points and local flooding points obtained in the ECT experiments are compared to global loading points and global flooding points obtained by measuring pressure drop and liquid hold-up to assess the CNN-aided ECT method performance.

A. *Bottom section of packed column flooding experiment*

1) *Real-time measurement of local liquid hold-up*

Real-time liquid distribution of structured packing obtained in previous studies using an ultrafast electron beam X-ray tomography technology indicated that the presence of packing in counter-current flow resulted in different scales of liquid maldistribution [16, 52]. Fig. 6 shows the ECT reconstructed images of the liquid distributions for the given gas flow rates. The maximum hold-up value in the liquid hold-up map is set to 100% for all results in order to have good contrast on pictures. Fig. 6 shows that the images at the bottom section clearly show liquid accumulation for gas superficial velocities higher than 4.49 m/s due to the liquid loading at the bottom of the column.

The ECT could monitor local liquid hold-up online without disrupting process operations and is, therefore, a preferable method to monitoring flooding. The local liquid hold-up values computed using the Maxwell equation are plotted against those measured using the level meter, as shown in Fig. 7. With a relative lower liquid hold-up (<13%), the Maxwell equation method predictions agreed with measurements to within 4%. With the increase of liquid hold-up, the Maxwell equation method suffers from large errors, showing an increasement in maximum error from 4% to 68% compared to the reference liquid hold-up. This level of agreement is likely not going to be satisfactory for packed column design. Those errors mainly come from the following two aspects: (a) linear simplification of Maxwell equation does not fit for the high liquid hold-up, and (b) high turbulent flow under flooding produces larger signal fluctuations. Therefore, a more accurate prediction method is desirable because adjustments of packings and solvents can lead to a higher value of liquid hold-up. In the following context, the proposed CNN-aided ECT technique is examined to acquire accurate liquid hold-up.

2) *Convolutional Neural Networks predicted local liquid hold-up*

In this subsection, the local liquid hold-up predicted by CNN is validated in the same way as the local liquid hold-up derived by the Maxwell equation, by comparing the reference local liquid hold-up measured with the level meter. Fig. 8 explicitly shows the results exhibit general linear relationships between the predicted liquid hold-up and the reference. By comparing Figs. 7 and 8, it is obvious that a significant improvement is obtained in the majority of cases, and such improvement becomes more obvious with liquid hold-up higher than 13%.

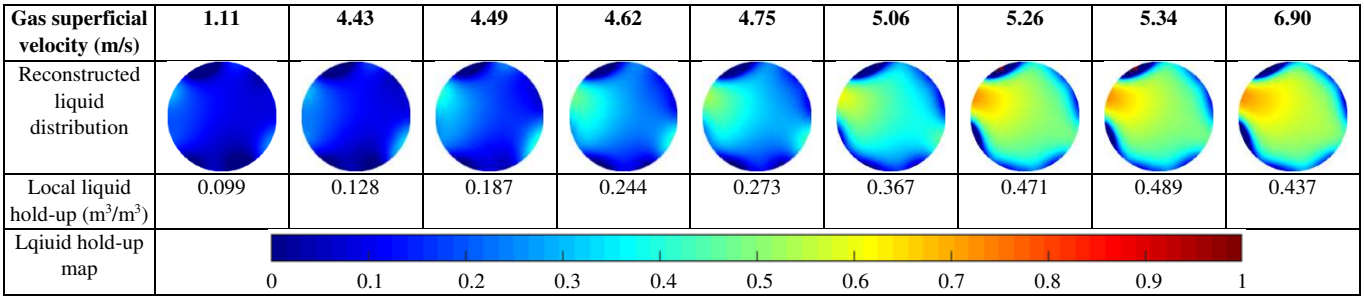

Fig. 6: Reconstructions of permittivity in a representative liquid hold-up distribution. Cross-sections of conductivity changes at the bottom (0 mm) of the packed column at given gas superficial velocities.

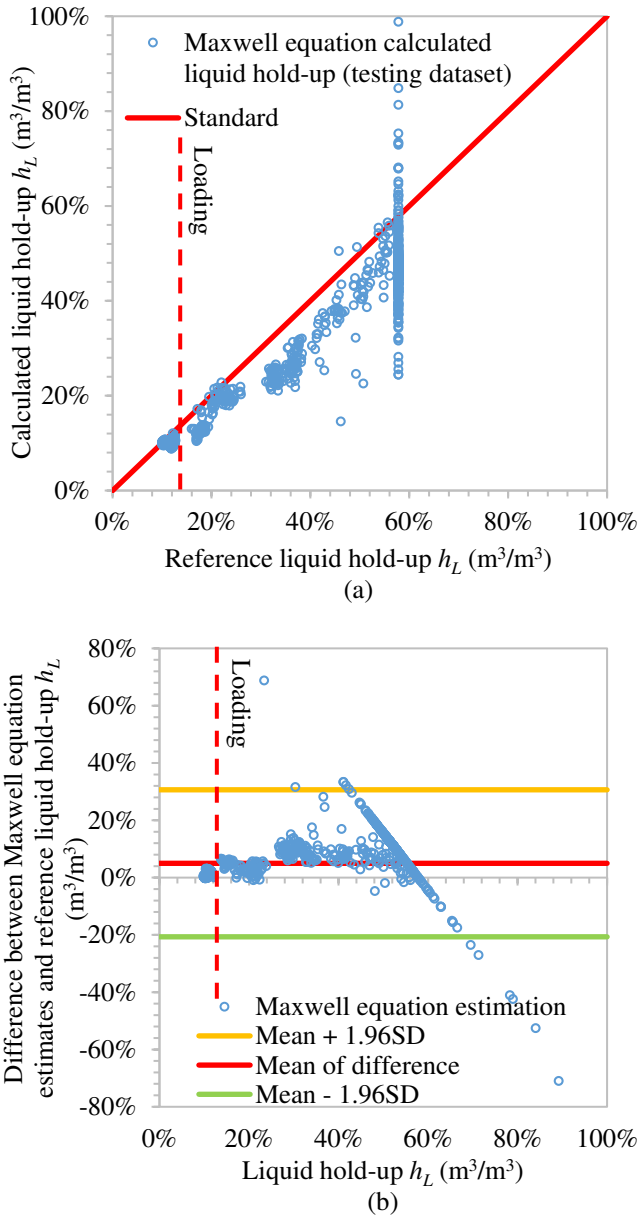

Fig. 7. At the bottom section of packed column, (a) Maxwell equation predicted local liquid hold-up and reference local liquid hold-up and (b) their differences.

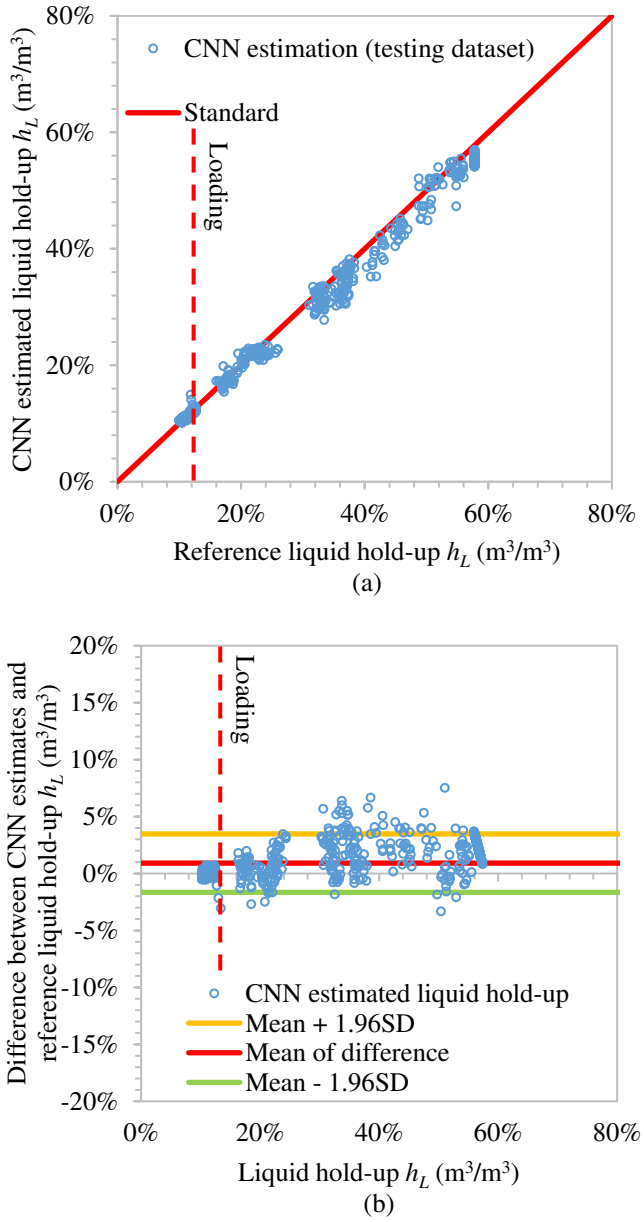

Fig. 8. At the bottom section of packed column, (a) CNN predicted local liquid hold-up and reference local liquid hold-up and (b) their differences.

The mean of difference and standard deviation of CNN predicted results is found to be 1% and 1.3% respectively, whereas for the Maxwell predicted results 5% and 13.1% respectively. The difference between the CNN estimates and the reference liquid hold-up shown in Fig. 8 (b) indicates that prediction results at low liquid hold-up are relatively more stable than results with high liquid hold-up. The divergence of the data from the expected linear relationship for a higher value of liquid hold-up (>13%) may be due to the high turbulent flow under flooding producing larger signal fluctuations.

3) Determination of Flooding

According to previous studies [53], loading points are established by a rapid increase in pressure drop and liquid hold-up. Loading could be identified visually through the transparent glass pipe, indicated by a turbulent layer of liquid accumulating at the bottom of the column, as shown in Fig. 9 (d). Flooding could also be identified visually through the transparent glass pipe, indicated by the entire column is filled with liquid and the high turbulent flow with a large amount of bubble going through the packing voids, as shown in Fig. 14 (d). The flooding point is identified visually when the top of the column is flooded. All these physical phenomena observed in the experiments are in agreement with the literature [14]. However, the loading or flooding points determined by visual observation could cause large errors [53]. In this study, the local loading point and global loading point are determined when the gradient

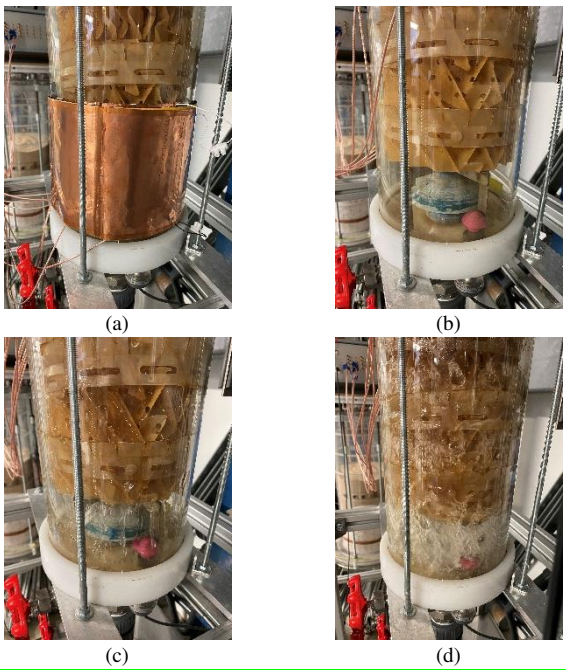

Fig. 9. Photos of bottom end packed column with (a) ECT sensor, (b) no flow, (c) non-flooding water flow, and (d) flooding and entrainment.

of each process variable reach a value above 10%. Results of global liquid hold-up and pressure drop are used to identify global loading point, whereas results of local liquid hold-up are used to identify local loading point. The earliest detection of the loading phenomenon will indicate the transition from pre-loading zone to loading zone. In the pre-loading zone, mass transfer efficiency is independent of flow rate. In the loading zone, liquid will start to accumulate or "load" at the bottom of the bed. Partial flooding could occur at higher gas rates in this zone to achieve maximum mass transfer efficiency.

4) Global loading point

In Fig. 10, the global liquid hold-up measured by the level meter is plotted against the gas superficial velocity at a specific liquid load of 21.17 m^3/m^3h. As the gas superficial velocity increases, the global liquid hold-up shows continual growth. The liquid hold-up of the entire column remains relatively constant until the gas flow velocity reaches 5.26 m/s. Beyond this point, a small increment of the gas flow results in a sharp increase of global liquid hold-up that reaches between 33.9% and 36.5% of liquid hold-up at 6.89 m/s. The global loading point is identified here as the gradient of global liquid hold-up measurements reaches 10%. In this instance, the global loading point occurs at a gas velocity ranging from 5.26 m/s to 5.34 m/s. After the global loading point, the curve maintains a clearly rising slope, indicating rapid accumulation of liquid in the column.

Typical results of pressure drop of the whole column are also shown with purple squares in Fig. 10. In the figure, the abscissa indicates the gas superficial velocity, while the secondary ordinate indicates the pressure drop. It can be seen that the general trend of the pressure drop curve is the same as the global liquid hold-up curve. The pressure drop of the entire column remains relatively constant until the gas flow reaches 5.26 m/s. Then, the pressure drop increases dramatically reaching values

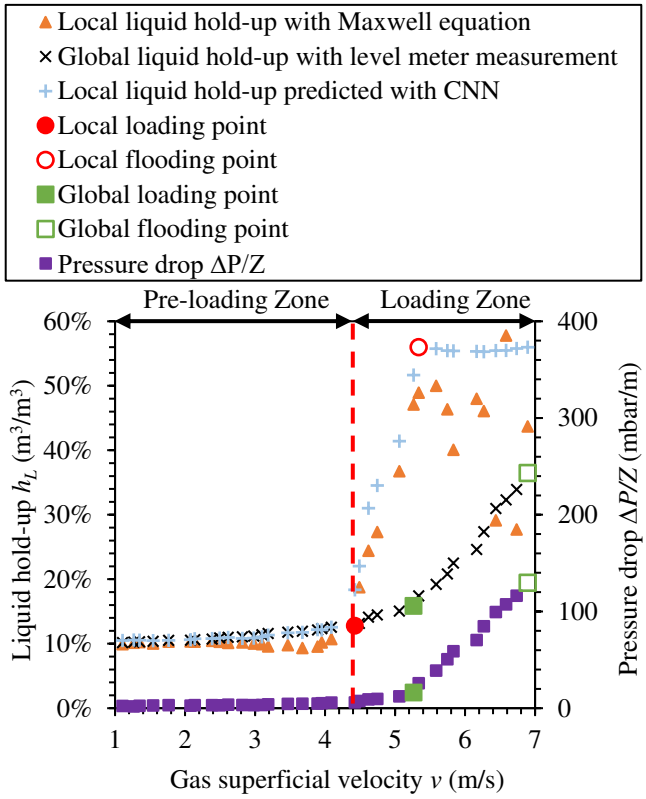

Fig. 10. Dependence of Maxwell equation and CNN predicted local liquid hold-up, level meter measured global liquid hold-up and pressure drop on gas superficial velocity.

between 116.2 mbar/m and 129.6 mbar/m at 6.89 m/s. In this case, the global loading point is identified where a rapid increase of gradient (>10%) occurs in the pressure drop curve. Green solid squares are used to indicate global loading point in Fig. 10. However, the loading point determined according to the gradient of the pressure drop and the global liquid hold-up did not match the observations, showing discrepancies of 19% slower than accumulation of liquid been observed. After the global loading point, the pressure drop curve maintains a positive slope, meaning that the accumulation of liquid reduces the cross-section area occupied by the gas phase and therefore accelerates the pressure drop rise. Green hollow squares are used to indicate global flooding point in Fig. 10, which was identified visually when top of the column is flooded.

5) Local loading point

Local liquid hold-up predicted by Maxwell equation and CNN is illustrated using the red triangle and sky blue cross lines on Fig. 10. Results from both methods are relatively consistent with global liquid hold-up in the pre-loading zone. Interestingly, in the pre-loading zone, the local liquid hold-up initially decreases from 10.9% to 9.3%, forming a minimum value, and then increases up to 57.8%. Prior studies also observed a similar phenomenon. A possible explanation is that the increase in gas flow breaks up the falling liquid film and causes liquid flow reversal [24, 45, 46].

The local liquid hold-up predicted with CNN remains relatively constant for gas velocities below 4.43 m/s, then increases dramatically to a plateau of 56%. The same local

loading point is identified with a rapid increase in local liquid hold-up calculated with Maxwell equation at 4.43 m/s gas flow, shown as the red solid point at 4.43 m/s. The local loading points determined according to the gradient of the local liquid hold-up matched very well with the observations. However, the gradient of the pressure drop and the global liquid hold-up with respect to gas velocity has no significant changes up to gas velocity of 5.26 m/s. These results indicate detection of localized loading can be achieved by ECT, at lower gas velocities than with conventional methods. After the local loading point, it can be seen that the plateau reaches maximum values between 55% and 56% with CNN and remains constant to the end of the experiment. The local flooding point, marked as red hollow point, is identified here as flooding was identified visually above the ECT. However, the Maxwell equation calculated local liquid hold-up at the plateau is very unstable at a range between 27.7% and 57.8%. The most important sources of experimental uncertainty have been discussed in Section II B.

To summarize this section, the occurrence of the local loading point can be detected using the ECT at the bottom of the column. The increase in liquid accumulation in the loading zone corresponds to an increase in high relative permittivity material (water), which is detected by the ECT. The direct comparison with pressure drop and global liquid hold-up with level meter measurement shows the validity of using ECT for the detection of liquid loading on packing.

B. Top section of packed column flooding experiment

1) Real-time measurement of local liquid hold-up

Similar to the experiments at the bottom section, Fig. 11 shows the image reconstruction of liquid distribution for the selected gas flow rates at the top section of the packed column. Images at the top section show liquid accumulation from 6.74 m/s gas superficial velocity due to the liquid loading from the base upwards. The results suggest that the distribution of liquid hold-up can be reconstructed, but the structural detail, such as small-scale maldistribution due to packing channels, cannot be observed in the images.

The liquid hold-up values calculated using the Maxwell equation, for gas flow rates from non-flooding to flooding, are plotted against those measured using the level meter, as shown in Fig. 12. Before the red doted loading line, the measured liquid hold-up agreed with the estimations of liquid hold-up to within 2%. Fig. 12 (b) shows that Maxwell equation estimations have the smallest relative error on samples before the red doted loading line, at about 10%, but the largest relative error on relative high liquid hold-up, at approximately 39%. This is a clear drawback of using the Maxwell equation to predict local liquid hold-up as the predicted results with large error after flooding onset occurs at the top section. The larger the liquid hold-up value is, the more significant deviation between the two measurements. Possible reasons for errors have been discussed in section V A (1).

2) Convolutional Neural Networks predicted liquid hold-up for flooding in packed column

The CNN predicted local liquid hold-up results are shown in Fig. 13. The results exhibit generally linear relationships between the CNN estimated liquid hold-up and reference liquid hold-up. The difference between CNN estimates and reference liquid hold-up in Fig. 13 (b) shows that lower liquid hold-up (<10%) are relatively more stable than higher liquid hold-up (>10%). By comparing Figs. 12 and 13, it is evident that a significant improvement is obtained in most cases, and such improvement becomes more obvious for the higher liquid hold-up (>10%). The mean of difference and standard deviation of CNN predicted results at the top section data sets was found to be 0.3% and 1.3%, whereas for the Maxwell predicted results 1% and 2.4%, respectively. These results indicate that the CNN model better predicts local liquid hold-up in the packed column, especially at high liquid hold-up.

3) Determination of flooding point

Similar to the experiments at the bottom section of the packed column, Fig. 15 show a comparison between the process variables such as pressure drop and liquid hold-up used for flooding prognosis. According to Billet and Schulets [6], the phenomenon of flooding includes liquid accumulation at the top of the bed. Our study uses experimental data sampled from the top section of the packed column to determine the local loading point as an early warning of flooding point, as shown in Fig. 15. Flooding can be identified visually through the transparent glass pipe because of a turbulent layer of liquid upon the top of the column. Therefore, the experiment is stopped when the flooding and entrainment are spotted at the top of the column, as shown in Fig. 14 (d).

Global liquid hold-up and global pressure drop are plotted for all the 35 air flow rates. It can be seen from Fig. 15 the overall trends of the pressure drop curve and global liquid hold-up curve are similar to those at the bottom section, under the same experimental conditions. Green solid square and are used to indicate global loading point. The global loading point is identified here as the gradient of global liquid hold-up and

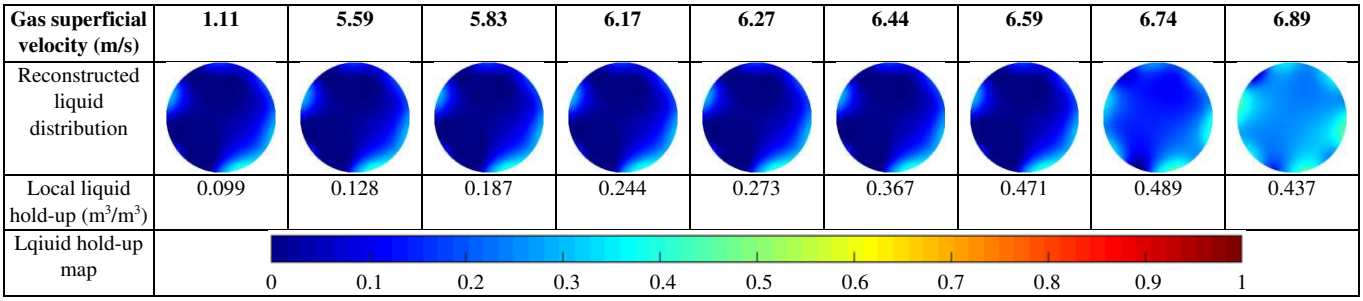

Fig. 11. Reconstructions of permittivity in a representative liquid hold-up distribution. Cross-sections of conductivity changes at the bottom (940 mm) of the packed column at given gas superficial velocities.

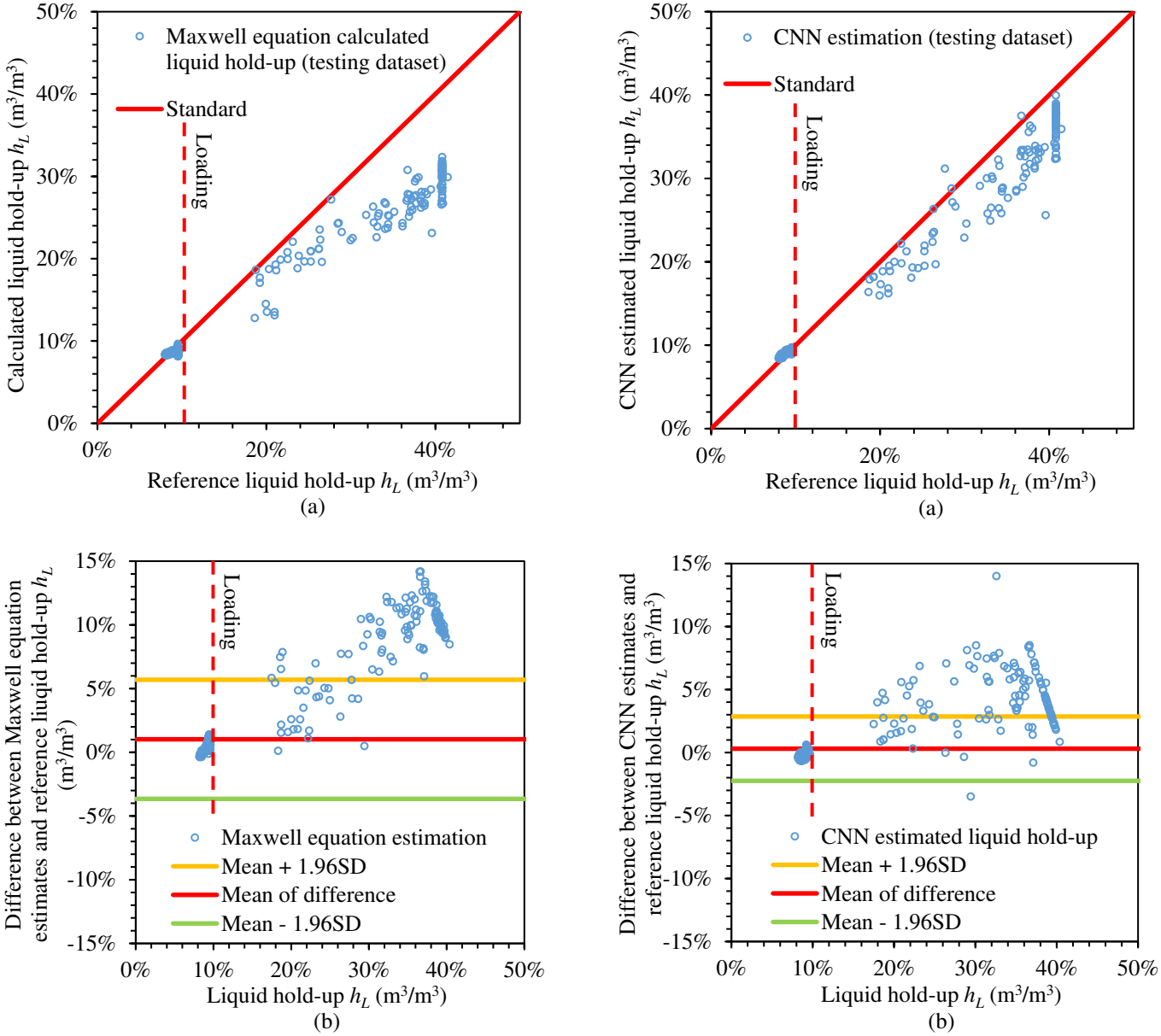

Fig. 12. At the top section of packed column, (a) Maxwell equation predicted local liquid hold-up and reference local liquid hold-up and (b) their differences.

Fig. 13. At the top section of packed column (a) CNN predicted local liquid hold-up and reference local liquid hold-up and (b) their differences.

pressure drop measurements has achieved a value of 10%. However, the gradient of pressure drop increases more rapidly than that at the bottom section. It is most likely that the pre-flooding causes this phenomenon by improving packing wetting degree.

As shown in Fig. 15, the Maxwell equation calculated local liquid hold-up and the CNN estimations range from 8.4% to 37.1% during the flooding experiment. In the pre-loading zone, a small change of the gradient of local liquid hold-up is observed at the top section of the packed column. Before the local loading point (marked as the red solid circle), no temporary accumulation of liquid at the top of the bed is observed. More importantly, the gas velocity does not affect the local liquid hold-up until the local loading point at the top is achieved. It can be concluded that the local liquid hold-up is independent of air flow rate, leading to low interfacial area and gas-liquid interactions at the top section [6]. The two curves show a very similar tendency, with a sharp rise observed when the flooding front has advanced up. The Maxwell equation predicted local liquid hold-up remains relatively constant until 6.59 m/s gas flow, then increases to a peak at approximately 6.89 m/s gas flow. In addition, the CNN predicted local liquid hold-up is relatively consistent with the Maxwell equation predicted ones and global liquid hold-up in the pre-flooding zone but increases much faster in the local flooding zone. The local liquid hold up may be underestimated using the Maxwell equation as the maximum liquid hold-up of 30.4% is much smaller than the global liquid hold-up, i.e., 37% at the same gas flow rate. In contrast, CNN estimations agree well with the global liquid hold-up close to the flooding point. The local

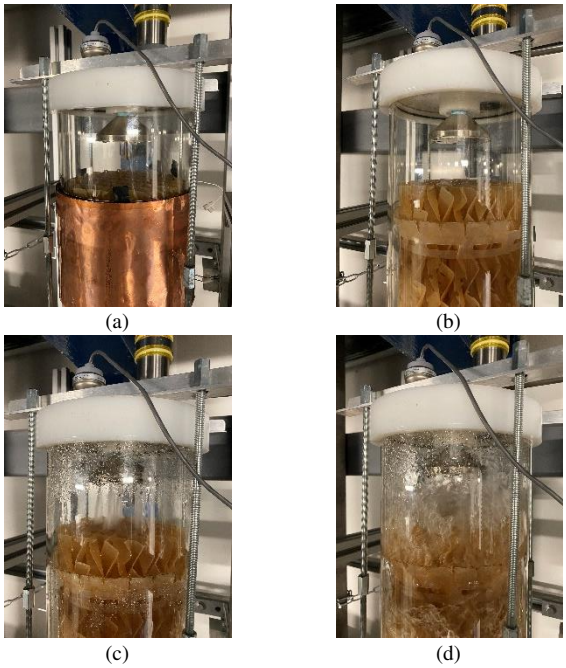

Fig. 14. Photos of top end packed column with (a) ECT sensor, (b) no flow, (c) non-flooding water flow, and (d) flooding and entrainment.

liquid hold-up profile demonstrates a rapid increase of gradient in Fig. 15 at around 37%, which signifies that the local loading point is found at approximately 6.59 m/s flow rate. Followed by a small increase of gas velocity, excessive entrainment at top of the column was observed at the experiment, which indicated gas velocity has also achieved global flooding point (marked as green hollow squares). Therefore, it can be concluded that the local liquid hold-up at the top section of the packed column can be used as the early warning of the flooding.

VI. Conclusion

This work presents the first attempt for Convolutional Neural Network-aided flooding prognostic in a packed column using Electrical Capacitance Tomography, with measurements of pressure drop, global liquid hold-up and Electrical Capacitance Tomography data. These process parameters were analysed and compared for flooding prognostic. The comparison among varying process variables shows that the local liquid hold-up estimated by Electrical Capacitance Tomography gives the earliest detection of loading point and early warning of flooding. The Maxwell method yields a mean of difference 5%, whilst the standard deviation of the mean of difference is 13.1%, implying the agreement is not consistent across all measurements. The results confirm that the estimates of local liquid hold-up are significantly affected by flooding. In contrast, a well-trained Convolutional Neural Network with a relatively large data set can predict the local liquid hold-up within 1% mean of difference and 1.3% standard deviation. The results under flooding conditions have verified the performance of the Convolutional Neural Network with the largest relative error of 8.5%.

These findings confirm that a local measurement of liquid hold-up tends to be the earliest prognostic of flooding than a global pressure drop or liquid hold-up. Electrical Capacitance

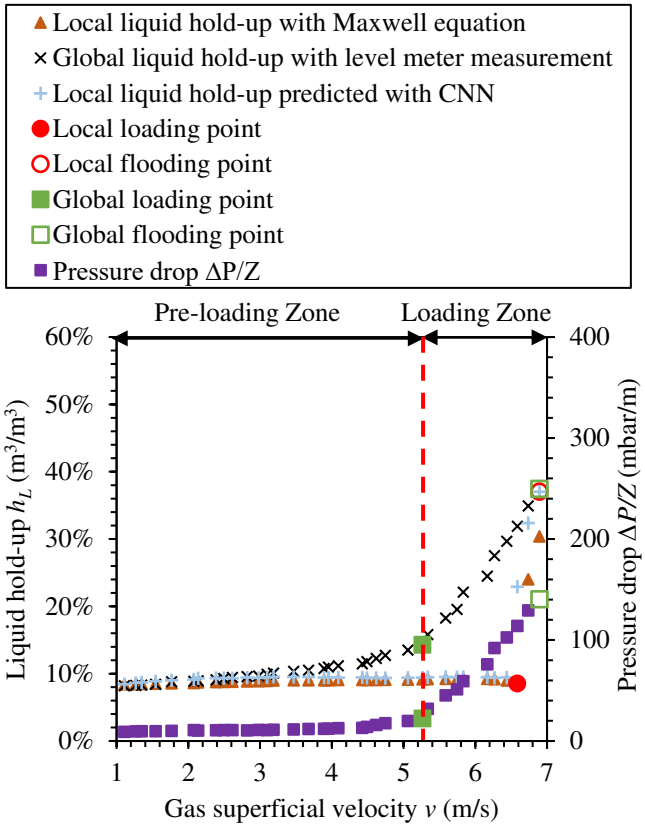

Fig. 15. Dependence of Maxwell equation and CNN predicted local liquid hold-up, level meter measured global liquid hold-up and pressure drop on gas superficial velocity.

Tomography with Convolutional Neural Network accurately predicts local liquid hold-up enabling the detection of loading point at the bottom of the packed column and the detection of the flooding point at the top of the packed column. It is therefore highly suitable for accurately predicting the occurrence of flooding and may be deployed in packed column operation to allow for the closer operation to the flooding point and reduce column size and capital costs.

References

[1] B. Sreenivasulu, D. Gayatri, I. Sreedhar, and K. Raghavan, "A journey into the process and engineering aspects of carbon capture technologies," *Renewable and Sustainable Energy Reviews,* vol. 41, pp. 1324-1350, 2015.

[2] D. Cann, C. Font-Palma, and P. Willson, "Experimental analysis of CO2 frost front behaviour in moving packed beds for cryogenic CO2 capture," *International journal of greenhouse gas control,* vol. 107, p. 103291, 2021.

[3] R. S. Haszeldine, "Carbon capture and storage: how green can black be?," *Science,* vol. 325, no. 5948, pp. 1647-1652, 2009.

[4] I. Fursule, K. Liu, and H. Nikolic, "Using the Carbon Capture Simulation Initiative (CCSI) Tool to Design the Experiments in the Parametric Campaign of a Novel Compact Absorber for Carbon Capture," Univ. of Kentucky, Lexington, KY (United States), 2020.

[5] E. Hansuld, L. Briens, and C. Briens, "Acoustic detection of flooding in absorption columns and trickle beds," *Chemical Engineering & Processing: Process Intensification,* vol. 47, no. 5, pp. 871--878, 2008.

[6] R. Billet and M. Schultes, "Prediction of mass transfer columns with dumped and arranged packings: updated summary of the calculation method of Billet and Schultes," *Chemical Engineering Research and Design,* vol. 77, no. 6, pp. 498-504, 1999.

[7] J. Maćkowiak, "Pressure drop in irrigated packed columns," *Chemical Engineering and Processing: Process Intensification,* vol. 29, no. 2, pp. 93-105, 1991.

[8] R. Billet, "Distillation engineering," 1979.

[9] M. Roustan, "Transferts gaz-liquide dans les procédés de traitement des eaux et des effluents gazeux," 2003.

[10] V. Wolf-Zöllner, F. Seibert, and M. Lehner, "Extended performance comparison of different pressure drop, hold-up and flooding point correlations for packed columns," *Chemical Engineering Research and Design,* vol. 147, pp. 699-708, 2019.

[11] Y. Taitel, D. Barnea, and A. Dukler, "A film model for the prediction of flooding and flow reversal for gas-liquid flow in vertical tubes," *International Journal of Multiphase Flow,* vol. 8, no. 1, pp. 1-10, 1982.

[12] J.-U. Repke, O. Villain, and G. Wozny, "A nonequilibrium model for three-phase distillation in a packed column: modelling and experiments," *Computers & chemical engineering,* vol. 28, no. 5, pp. 775-780, 2004.

[13] P. Amani, J. Safdari, H. Abolghasemi, M. H. Mallah, and A. Davari, "Two-phase pressure drop and flooding characteristics in a horizontal-vertical pulsed sieve-plate column," *International Journal of Heat and Fluid Flow,* vol. 65, pp. 266-276, 2017.

[14] J. Maćkowiak, "Determination of flooding gas velocity and liquid hold-up at flooding in packed columns for gas/liquid systems," *Chemical engineering & technology,* vol. 13, no. 1, pp. 184-196, 1990.

[15] R. Caulkin, M. Fairweather, X. Jia, N. Gopinathan, and R. A. Williams, "An investigation of packed columns using a digital packing algorithm," *Computers & chemical engineering,* vol. 30, no. 6, pp. 1178-1188, 2006.

[16] M. Fourati, V. Roig, and L. Raynal, "Experimental study of liquid spreading in structured packings," *Chemical Engineering Science,* vol. 80, pp. 1-15, 2012.

[17] K. Groß *et al.*, "Analysis of Flow Patterns in High-Gravity Equipment Using Gamma-Ray Computed Tomography," *Chemie ingenieur technik,* vol. 91, no. 7, pp. 1032-1040, 2019.

[18] Y. Yang *et al.*, "A noninvasive X-ray technique for determination of liquid holdup in a rotating packed bed," *Chemical engineering science,* vol. 138, pp. 244-255, 2015.

[19] S. Maurer *et al.*, "Correlating bubble size and velocity distribution in bubbling fluidized bed based on X-ray tomography," *Chemical engineering journal (Lausanne, Switzerland : 1996),* vol. 298, pp. 17-25, 2016.

[20] Z. Zeeshan, C. E. Zuccarelli, D. Ospina Acero, Q. M. Marashdeh, and F. L. Teixeira, "Enhancing Resolution of Electrical Capacitive Sensors for Multiphase Flows by Fine-Stepped Electronic Scanning of Synthetic Electrodes," *IEEE transactions on instrumentation and measurement,* vol. 68, no. 2, pp. 462-473, 2019.

[21] L. Zhu, L. Ma, Y. Li, Y. Yang, and M. Zhang, "Linearization Point and Frequency Selection for Complex-Valued Electrical Capacitance Tomography," *IEEE transactions on instrumentation and measurement,* vol. 70, pp. 1-11, 2021.

[22] A. Wongkia, F. Larachi, and S. Assabumrungrat, "Hydrodynamics of countercurrent gas–liquid flow in inclined packed beds – A prospect for stretching flooding capacity with small packings," *Chemical Engineering Science,* vol. 138, pp. 256--265, 2015.

[23] D. Strazza, M. Demori, V. Ferrari, and P. Poesio, "Capacitance sensor for hold-up measurement in high-viscous-oil/conductive-water core-annular flows," *Flow measurement and instrumentation,* vol. 22, no. 5, pp. 360-369, 2011.

[24] S. H. Stavland, Y. Arellano, A. Hunt, R. Maad, and B. T. Hjertaker, "Multimodal Two-Phase Flow Measurement Using Dual Plane ECT and GRT," *IEEE transactions on instrumentation and measurement,* vol. 70, pp. 1-12, 2021.

[25] S. Sun, X. Lu, L. Xu, Z. Cao, J. Sun, and W. Yang, "Real-Time 3-D Imaging and Velocity Measurement of Two-Phase Flow Using a Twin-Plane ECT Sensor," *IEEE transactions on instrumentation and measurement,* vol. 70, pp. 1-10, 2021.

[26] M. Hamidipour and F. Larachi, "Characterizing the liquid dynamics in cocurrent gas–liquid flows in porous media using twin-plane electrical capacitance tomography," *Chemical Engineering Journal,* vol. 165, no. 1, pp. 310-323, 2010.

[27] B. Matusiak, M. J. da Silva, U. Hampel, and A. Romanowski, "Measurement of dynamic liquid distributions in a fixed bed using electrical capacitance tomography and capacitance wire-mesh sensor," *Industrial & engineering chemistry research,* vol. 49, no. 5, pp. 2070-2077, 2010.

[28] R. B. White, "Using electrical capacitance tomography to monitor gas voids in a packed bed of solids," *Measurement science and technology,* vol. 13, no. 12, p. 1842, 2002.

[29] Z. Li, Y. Chen, Y. Yang, C. Liu, M. Lucquiaud, and J. Jia, "Flow regime transition in countercurrent packed column monitored by ECT," *Chemical engineering journal,* vol. 420, p. 129841, 2021.

[30] J. Zheng, J. Li, Y. Li, and L. Peng, "A Benchmark Dataset and Deep Learning-Based Image Reconstruction for Electrical Capacitance Tomography," *Sensors (Basel, Switzerland),* vol. 18, no. 11, pp. 3701-, 2018.

[31] Z. Chen, J. Xiang, P.-O. Bagnaninchi, and Y. Yang, "MMV-Net: A Multiple Measurement Vector Network for Multifrequency Electrical Impedance Tomography," *IEEE Transactions on Neural Networks and Learning Systems,* 2022.

[32] G. Kłosowski, T. Rymarczyk, K. Niderla, M. Rzemieniak, A. Dmowski, and M. Maj, "Comparison of Machine Learning Methods for Image Reconstruction Using the LSTM Classifier in Industrial Electrical Tomography," *Energies,* vol. 14, no. 21, p. 7269, 2021.

[33] A. Jaworski and G. Bolton, "The design of an electrical capacitance tomography sensor for use with media of high dielectric permittivity," *Measurement Science and Technology,* vol. 11, no. 6, p. 743, 2000.

[34] K. Zainal-Mokhtar and J. Mohamad-Saleh, "An oil fraction neural sensor developed using electrical capacitance tomography sensor data," *Sensors,* vol. 13, no. 9, pp. 11385-11406, 2013.

[35] H. Wang and L. Zhang, "Identification of two-phase flow regimes based on support vector machine and electrical capacitance tomography," *Measurement Science and Technology,* vol. 20, no. 11, p. 114007, 2009.

[36] M. Hasan, S. Ullah, M. J. Khan, and K. Khurshid, "Comparative analysis of SVM, ANN and CNN for classifying vegetation species using hyperspectral thermal infrared data," *The International Archives of Photogrammetry, Remote Sensing and Spatial Information Sciences,* vol. 42, pp. 1861-1868, 2019.

[37] J. Zheng, H. Ma, and L. Peng, "A CNN-based image reconstruction for electrical capacitance tomography," in *2019 IEEE International Conference on Imaging Systems and Techniques (IST)*, 2019: IEEE, pp. 1-6.

[38] C. Gunes, Q. M. Marashdeh, and F. L. Teixeira, "A Comparison Between Electrical Capacitance Tomography and Displacement-Current Phase Tomography," *IEEE sensors journal,* vol. 17, no. 24, pp. 8037-8046, 2017.

[39] D. Hu, K. Lu, and Y. Yang, "Image reconstruction for electrical impedance tomography based on spatial invariant feature maps and convolutional neural network," in *2019 IEEE International Conference on Imaging Systems and Techniques (IST)*, 2019: IEEE, pp. 1-6.

[40] M. A. Rodriguez-Frias and W. Yang, "Dual-modality 4-terminal electrical capacitance and resistance tomography for multiphase flow monitoring," *IEEE Sensors Journal,* vol. 20, no. 6, pp. 3217-3225, 2019.

[41] W. Yang and L. Peng, "Image reconstruction algorithms for electrical capacitance tomography," *Measurement science and technology,* vol. 14, no. 1, p. R1, 2002.

[42] J. Jia, M. Wang, and Y. Faraj, "Evaluation of EIT Systems and Algorithms for Handling Full Void Fraction Range in Two-phase Flow Measurement," 2014.

[43] Y. Yang, L. Peng, and J. Jia, "A novel multi-electrode sensing strategy for electrical capacitance tomography with ultra-low dynamic range," *Flow Measurement and instrumentation,* vol. 53, pp. 67-79, 2017.

[44] H. Wu *et al.*, "Liquid distribution and hold-up measurement in counter current flow packed column by electrical capacitance tomography," *Chemical Engineering Journal,* vol. 353, pp. 519-532, 2018.

[45] Y. Li *et al.*, "Gas/oil/water flow measurement by electrical capacitance tomography," *Measurement science & technology,* vol. 24, no. 7, p. 74001, 2013.

[46] C. g. Xie, "Measurement Of Multiphase Flow Water Fraction And Water-cut," in *AIP Conference Proceedings*, 2007, vol. 914, no. 1: American Institute of Physics, pp. 232-239.

[47] Y. LeCun, Y. Bengio, and G. Hinton, "Deep learning," *nature,* vol. 521, no. 7553, pp. 436-444, 2015.

[48] S. Parthasarathy, H. Gowan, and P. Indhar, "Prediction of flooding in an absorption column using neural networks," in *Proceedings of the 1999 IEEE International Conference on Control Applications (Cat. No. 99CH36328)*, 1999, vol. 2: IEEE, pp. 1056-1061.

[49] W. Yang, "Design of electrical capacitance tomography sensors," *Measurement science & technology,* vol. 21, no. 4, p. 042001, 2010.

[50] K. P. Murphy, *Machine learning: a probabilistic perspective*. MIT press, 2012.

[51] A. Ousaka, A. Kariyasaki, and T. Fukano, "Prediction of flooding gas velocity in gas–liquid counter-current two-phase flow in inclined pipes," *Nuclear engineering and design,* vol. 236, no. 12, pp. 1282-1292, 2006.
[52] P. Marchot, D. Toye, M. Crine, A. M. Pelsser, and G. L'homme, "Investigation of Liquid Maldistribution in Packed Columns by X-Ray Tomography," *Chemical Engineering Research and Design,* vol. 77, no. 6, pp. 511--518, 1999.
[53] P. A. Schweitzer, "Handbook of separation techniques for chemical engineers/editor in chief, Philip A. Schweitzer."